



Reusable PdO/Al₂O₃–Nd₂O₃ photocatalysts in the UV photodegradation of phenol

A. Barrera ^{a,*}, F. Tzompantzi ^b, J.M. Padilla ^a, J.E. Casillas ^a, G. Jácome-Acatitla ^b, M.E. Cano ^a, R. Gómez ^b

^a Universidad de Guadalajara, Centro Universitario de la Ciénega, Laboratorio de Nanomateriales Catalíticos, Av. Universidad, Número 1115, Col. Linda Vista, C.P. 47820, Ocotlán, Jalisco, Mexico

^b Universidad Autónoma Metropolitana – Iztapalapa, Departamento de Química, San Rafael Atlixco No. 186, México 09340, D.F., Mexico

ARTICLE INFO

Article history:

Received 8 January 2013

Received in revised form 3 July 2013

Accepted 9 July 2013

Available online 17 July 2013

Keywords:

PdO photocatalysts

Al₂O₃–Nd₂O₃

Sol–Gel

Photodegradation

Phenol

ABSTRACT

The UV photodegradation of phenol in aqueous medium using PdO supported on binary Al₂O₃–Nd₂O₃ oxides as photocatalysts was studied. The PdO/Al₂O₃–Nd₂O₃ photocatalysts were prepared by the sol–gel method and characterized by N₂ physisorption, XRD, Raman spectroscopy and UV–vis diffuse reflectance spectroscopy. Bare PdO/γ-Al₂O₃ was found active for the photodegradation of phenol in aqueous medium. However, the addition of Nd₂O₃ to the γ-Al₂O₃ improves the photocatalytic activity of PdO photocatalysts as well as the decrease of dissolved organic carbon in aqueous milieu. Highest photocatalytic activity of PdO photocatalysts was observed for 10 wt% of Nd₂O₃ added to the γ-Al₂O₃ increasing the activity by a factor of two with respect to that of PdO/γ-Al₂O₃ after six hours of irradiation. The photocatalytic activity in the degradation of phenol by using the recovered PdO/Al–Nd photocatalysts is preserved after reaction.

© 2013 Elsevier B.V. All rights reserved.

1. Introduction

Phenol is a highly toxic compound that causes environmental pollution and is found in waste waters coming from various industrial processes such as petroleum refining, paper processing, resin and plastic production, carbon liquefaction, and pharmaceutical industry. Many research efforts have been devoted to develop methods for eliminating this compound from soil and water by means of biological and physical–chemical methods. Regarding the latter, increased attention has been paid nowadays to the application of photocatalysis using UV irradiation as an advanced oxidation processes for eliminating organic pollutants such as phenol in aqueous wastes using semiconductor materials as photocatalysts [1–3]. In this way photocatalytic materials like TiO₂ [4–6], Fe(III) carboxylates complexes [7–9], and layered double hydroxides [10–12] have been tested for the photodegradation of phenols in aqueous medium. Alternative combination using noble metal oxides as co-catalysts of alumina modified with rare earth oxides have been recently reported as interesting photodegradation catalysts of pesticides like 2, 4-D [13]. Palladium oxide (PdO) is a p-type semiconductor and it is of technological interest to use it as co-catalyst

since it has been reported as an efficient photocathode in the water electrolysis [14], however, to our knowledge the use of PdO supported on γ-Al₂O₃ as a photocatalyst for the photodegradation of phenol has not been reported before. Neodymium oxide has been reported as a stabilizer of γ-Al₂O₃ surface area [15,16] and it was used as doping agent for titania semiconductors for photocatalytic purposes [17–21]. It should be of outmost interest to investigate the photocatalytic activity of PdO supported on Al₂O₃–Nd₂O₃ for the photodegradation of phenol in aqueous medium. It is well known that the physicochemical properties of lanthanide-doped alumina materials depend on the method of preparation used and, as common as it is known, the sol–gel method is the most attractive one since it allows the synthesis of homogeneous mixed oxides with high specific surface area [17,22–27]. With this purpose, in order to study the stability of PdO/Al₂O₃–Nd₂O₃ photoactive materials, in the present work the photodegradation of phenol in aqueous medium is reported. For the characterization of the materials, methods such as N₂ physisorption, XRD, Raman spectroscopy and UV–vis diffuse reflectance spectroscopy are used.

2. Experimental methods

2.1. Preparation of 1 wt% PdO/Al₂O₃–Nd₂O₃ photocatalysts

Al₂O₃–Nd₂O₃ binary oxides (Al–Nd-x, where x = 2, 5, and 10 wt% of Nd₂O₃) were synthesized by the sol–gel method following

* Corresponding author. Tel.: +52 392 92 594 00; fax: +52 392 92 540 30.

E-mail addresses: arturo.barrera@cuci.udg.mx, arturobr2003@yahoo.com.mx (A. Barrera).

the method reported previously [13], in brief: aluminum tri-sec-butoxide (Alfa Aesar) was dissolved in a three mouth glass flask containing 10 mL of 2-methylpentane 2,4-diol (JT Baker) as a complexing agent at 70 °C and stirring for 1 h. After cooling down to 50 °C, the required amount of neodymium acetylacetone (Alfa Aesar) dissolved previously in acetone at 40 °C for 1 h was added to the flask containing the aluminum precursor. Then, approximately 10 mL of deionized water was added to the solution drop wise to carry out the alkoxide hydrolysis. The obtained gels were aged at 55 °C for 2 h and then at 80 °C during 12 h. After that, the solids were dried in an oven at 110 °C for 12 h followed by calcination under static air at 650 °C for 4 h. Bare Al₂O₃ (Al) was prepared following the method described before but without adding neodymium acetylacetone. Calcined Al, and Al-Nd-x binary oxides were impregnated with a PdCl₂ (Aldrich) aqueous solution in appropriated amounts to obtain catalysts with 1.0 wt% of PdO. The impregnated solids were dried at 110 °C for 12 h and then calcined in an oven at 650 °C for 3 h and labelled as PdO/Al₂O₃ (PdO/Al) and 1.0 wt% PdO/Al₂O₃–Nd₂O₃ (PdO/Al–Nd-x, where x = 2, 5, 10 wt% of Nd₂O₃).

2.2. Characterization of 1 wt% PdO/Al₂O₃–Nd₂O₃ photocatalysts

The textural properties of PdO photocatalysts were determined by nitrogen physisorption at –195.6 °C by using an Autosorb system (IQ model from Quantachrome). Before measurements, samples were flushed with Ar at 200 °C for 3 h. Specific surface area was determined from the nitrogen adsorption isotherms using the Brunauer–Emmet–Teller (BET) equation. Pore size distributions were calculated according to the Barrett, Joyner and Halenda (BJH) method by using the desorption branch of nitrogen isotherms.

XRD powder diffraction patterns of PdO/Al₂O₃–Nd₂O₃ photocatalysts were recorded at room temperature with a Bruker D-8 Advance diffractometer with the Bragg–Brentano geometry, using a Cu K α ($\lambda = 0.154$ nm) radiation source, a Ni 0.5% Cu-K β -filter in the secondary beam, and a 1-dimensional position sensitive silicon strip detector (Bruker, Linxeye). The diffraction intensity as a function of the angle 2θ was measured between 20° and 110°, with a 2θ step of 0.01945°, for 53 s per point. Identification of the diffraction peaks from the XRD patterns was carried out using the JCPDS database. X-ray diffraction patterns of PdO photocatalysts were also measured in the angle range of $2\theta = 30$ –44° at a scan rate of 10 min per step in order to improve the resolution of diffraction peaks in this range. X-ray diffraction patterns of some samples were also obtained from the recovered solids by drying the remaining aqueous phenol – photocatalyst dissolution after 6 h of UV irradiation.

Raman spectra of PdO photocatalysts were recorded in the 100–3500 cm^{–1} wavenumber range by using a Raman DXR Thermo Scientific Microscope equipped with an Nd:YVO₄DPSS laser source. The excitation line of the laser was 532 nm and the laser power was 10 mW.

UV-vis diffuse reflectance spectra of PdO photocatalysts were recorded in a UV-vis CARY 100 SCAN spectrometer with a scan speed of 600 nm min^{–1} with intervals of data collection of 1 nm and a change of the light source at a wavelength of 350 nm.

2.3. Photocatalytic degradation of phenol

The phenol photocatalytic degradation was carried out by using a batch-type round bottom cylindrical glass photoreactor of 1 L surrounded by a double-wall glass jacket. Previous to the photodegradation experiments, an aqueous solution of phenol (99.9%, Sigma–Aldrich) with a concentration of 0.86 mmol L^{–1} (80 ppm) was bubbled with air during 2 h. After that, 200 mL of the phenol solution was put into the glass photoreactor followed by the

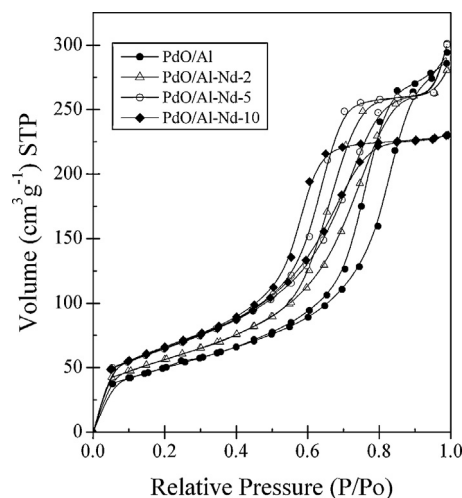


Fig. 1. Nitrogen adsorption–desorption isotherms of PdO photocatalysts supported on γ -Al₂O₃ and Al₂O₃–Nd₂O₃ binary oxides.

addition of 200 mg of the photocatalyst to give a concentration of 1 mg of photocatalyst per mL of phenol solution. Some selected photocatalyst samples were also tested in the photodegradation of phenol at concentrations of 0.25, 0.5, 1.0 and 1.5 g of photocatalyst sample per liter of phenol solution in order to study the effect of photocatalyst weight on the photocatalytic activity. Under continuous aeration (1 mL/s) and stirring, the phenol solution was then irradiated with a Pen-Ray UV power supply lamp (UVP products) with a typical wavelength of 254 nm and intensity of 4400 μ W cm^{–2} immersed into the solution using a protected quartz tube. Prior to the photocatalytic experiments, the aqueous phenol dissolution and the catalyst were kept in contact for 1 h without irradiation in order to determine the adsorption capacity of the solids. Then, the UV lamp was turned on. Samples of the irradiated dissolution were taken out from the photoreactor and filtered each hour for a period of 6 h in order to follow the photodegradation of phenol as a function of time. The phenol degradation was followed by UV-vis spectroscopy, employing a CARY 100 spectrophotometer and measuring the absorbance at $\lambda = 270$ nm. After irradiation, the solids were recovered and dried at 80 °C for 12 h and then analyzed by XRD.

The amount of dissolved organic carbon (DOC) during the photocatalytic experiments was followed using a TOC-V_{CEN} Shimadzu 5000 analyzer (catalytic oxidation on Pt at 680 °C). Calibration runs were performed injecting known amounts of potassium phthalate.

3. Results and discussion

3.1. Porous texture of Pd/Al₂O₃–Nd₂O₃ photocatalysts

Fig. 1 shows the nitrogen adsorption–desorption isotherms of PdO photocatalysts supported on Al₂O₃–Nd₂O₃ binary oxides prepared by the sol–gel method. Isotherms of PdO/Al and PdO/Al–Nd-x photocatalysts are of type IV which is typical of mesoporous materials with a hysteresis loop changing with the Nd₂O₃ concentration from the H1-type to the H2-type according to the IUPAC classification [28]. The variation in the hysteresis loop indicates that the form of the pores changes with the Nd₂O₃ concentration from well-defined cylindrical-like pores or agglomerates of compacts of uniform spheres in the PdO/Al photocatalyst into not well-defined shape pores with pore blocking effects that is typical of disordered materials in the PdO/Al–Nd-10 photocatalyst. The form of the pore size distributions is also modified with the Nd₂O₃ concentration in the binary oxide supports (**Fig. 2**). The pore size distributions of

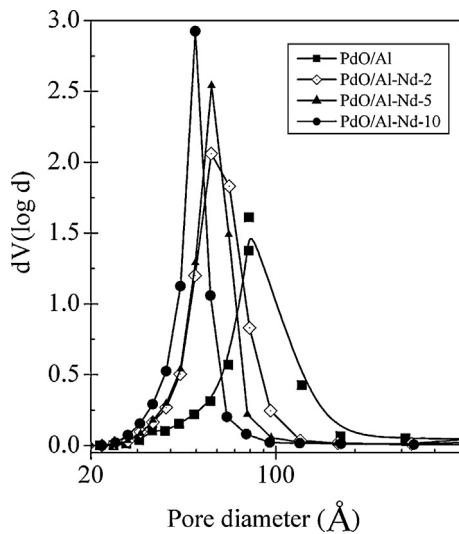


Fig. 2. Pore-size distributions of PdO photocatalysts supported on $\gamma\text{-Al}_2\text{O}_3$ and $\text{Al}_2\text{O}_3\text{-Nd}_2\text{O}_3$ binary oxides.

Table 1
Textural properties of $\text{PdO/Al}_2\text{O}_3\text{-Nd}_2\text{O}_3$ photocatalysts.

Catalyst ^a	S_{BET} ($\text{m}^2 \text{ g}^{-1}$)	V_{PT} ($\text{cm}^3 \text{ g}^{-1}$)	MPD (\AA)
PdO/Al	214.0	0.40	75
PdO/Al-Nd-2	242.0	0.44	57
PdO/Al-Nd-5	248.0	0.47	57
PdO/Al-Nd-10	259.0	0.50	50

^a The number in the code means the wt% of Nd_2O_3 .

PdO/Al and PdO/Al-Nd-2 photocatalysts are wide, whereas the pore size distributions of PdO/Al-Nd-5 and PdO/Al-Nd-10 photocatalysts are narrow and sharp. The pore diameter of maximum peak (MPD) is modified with Nd_2O_3 concentration decreasing from 80 \AA in the pore size distribution of the PdO/Al photocatalyst to 50 \AA in the PdO/Al-Nd-10 photocatalyst (Table 1). The specific surface area (S_{BET}) of PdO photocatalysts is improved with Nd_2O_3 concentration in the $\text{Al}_2\text{O}_3\text{-Nd}_2\text{O}_3$ binary oxides (Table 1); the S_{BET} of the PdO/Al photocatalyst is $214 \text{ m}^2 \text{ g}^{-1}$, whereas the S_{BET} of the PdO/Al-Nd-10 photocatalyst increases to a value of $259 \text{ m}^2 \text{ g}^{-1}$. It means that the S_{BET} is improved about 21% when 10 wt% of Nd_2O_3 is added to the alumina support by the sol-gel method. The increase in the S_{BET} of PdO/Al-Nd-x photocatalysts with Nd_2O_3 concentration suggests that the Nd_2O_3 acts as a textural promoter of the alumina. Moreover, the total specific pore volume (V_{PT}) of PdO photocatalysts is also increased with Nd_2O_3 concentration in the binary oxides. The V_{PT} of PdO/Al-Nd-10 photocatalyst is improved about 25% with respect to that of PdO/Al (Table 1).

3.2. Crystalline structure of $\text{Pd/Al}_2\text{O}_3\text{-Nd}_2\text{O}_3$ photocatalysts

XRD patterns of PdO photocatalysts supported on $\text{Al}_2\text{O}_3\text{-Nd}_2\text{O}_3$ binary oxides (Fig. 3) show the presence of $\gamma\text{-Al}_2\text{O}_3$ as evidenced by the diffraction peaks at $2\theta = 19.4^\circ, 37.5^\circ, 39.6^\circ, 45.9^\circ, 60.5^\circ$ and 66.8° corresponding to the (1 1 1), (3 1 1), (2 2 2), (4 0 0), (5 1 1) and (4 4 0) planes of the $\gamma\text{-Al}_2\text{O}_3$ (29-63, 10-425 JCPDS) [13]. In addition, some small diffraction peaks at $2\theta = 33.8^\circ$ and 54.95° corresponding to the (1 0 1) and (1 1 2) planes of the PdO tetragonal phase (00-041-1107 JCPDS) are also observed in the XRD patterns. The presence of tetragonal PdO is also confirmed by Raman spectroscopy (Fig. 4) where the Raman shift peak observed at 650 cm^{-1} in the Raman spectra of PdO/Al and of PdO/Al-Nd-x is assigned to the B_{1g} Raman mode of crystalline PdO [14]. The diffraction peak at $2\theta = 33.8^\circ$ is clearly observed when the XRD patterns are

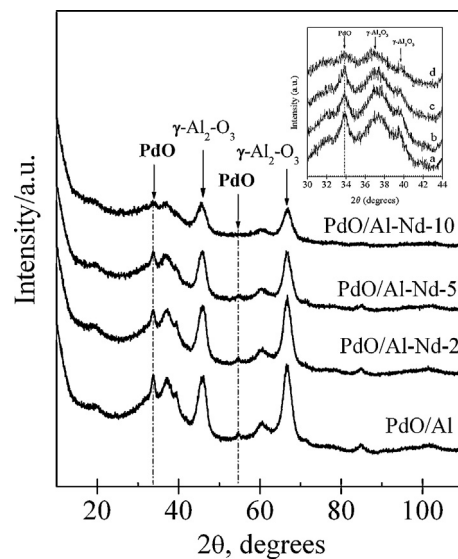


Fig. 3. X-ray diffraction patterns of PdO photocatalysts supported on $\gamma\text{-Al}_2\text{O}_3$ and $\text{Al}_2\text{O}_3\text{-Nd}_2\text{O}_3$ binary oxides. Inset plot: XRD patterns measured at low scan rate in the $2\theta = 30\text{--}44^\circ$ range: (a) PdO/Al; (b) PdO/Al-Nd-2; (c) PdO/Al-Nd-5; and (d) PdO/Al-Nd-10.

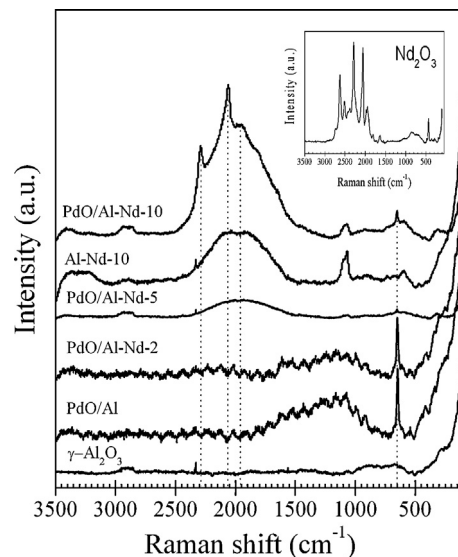


Fig. 4. Raman spectra of $\gamma\text{-Al}_2\text{O}_3$, Al-Nd-10 binary oxide and PdO photocatalysts supported on $\gamma\text{-Al}_2\text{O}_3$ and $\text{Al}_2\text{O}_3\text{-Nd}_2\text{O}_3$ binary oxides. Inset plot: Raman spectra of Nd_2O_3 .

obtained at a lower scanning rate in the range $30\text{--}44^\circ$ (inset in Fig. 3). As the neodymium oxide concentration in the binary oxides is increased, a decrease in the intensity as well as the widening of PdO and $\gamma\text{-Al}_2\text{O}_3$ diffraction peaks is observed in the XRD patterns suggesting the decrease in their crystallite sizes due to interaction effects with Nd_2O_3 . Such decrease in the crystallite sizes of $\gamma\text{-Al}_2\text{O}_3$ with the increase in the Nd_2O_3 concentration in the Al-Nd-x binary oxides should explain the improvement in the S_{BET} of the PdO/Al-Nd-x photocatalysts. On the other hand, not every diffraction peak corresponding to the Nd_2O_3 phase is observed in the XRD patterns of PdO/Al-Nd-x photocatalysts suggesting that neodymium oxide species are highly dispersed as small nano-crystalline domains that are randomly well-mixed with the $\gamma\text{-Al}_2\text{O}_3$ agglomerates. In spite of that not every diffraction peak belonging to Nd_2O_3 is detected by XRD; however, their presence is inferred by Raman spectroscopy where the Raman shift peaks

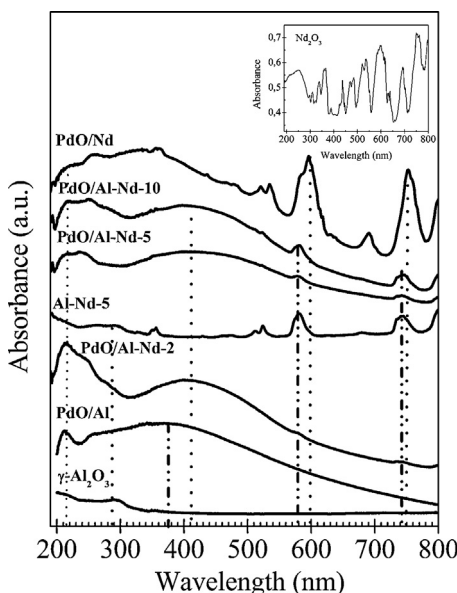


Fig. 5. UV-vis spectra of $\gamma\text{-Al}_2\text{O}_3$, Al-Nd-5 binary oxide and PdO photocatalysts supported on $\gamma\text{-Al}_2\text{O}_3$, Nd₂O₃ and Al₂O₃-Nd₂O₃ binary oxides. Inset plot: UV-vis spectra of Nd₂O₃.

observed at 1950, 2060 and 2280 cm⁻¹ in the spectra of PdO/Al-Nd-10 (Fig. 4) are attributed to Nd₂O₃ transitions. This asseveration is done since these Raman shift peaks are not present in the Raman spectra of $\gamma\text{-Al}_2\text{O}_3$ or PdO/ $\gamma\text{-Al}_2\text{O}_3$, but they are consistent with the Raman spectra of Al-Nd-10 binary oxide and Nd₂O₃ (inset in Fig. 4). These Raman shift peaks are absent in the Raman spectra of the PdO/Al-Nd-2 photocatalyst confirming that neodymium oxide is highly dispersed as small nano-crystallites within the $\gamma\text{-Al}_2\text{O}_3$ agglomerates. However, at higher neodymium oxide concentration (PdO/Al-Nd-5), the Raman spectra shows the appearance of a wide Raman shift peak of low intensity in the 1500–2500 cm⁻¹ range. This wide Raman shift peak corresponds to Nd₂O₃ transitions as can be seen by comparison with the Raman spectra of PdO/Al-Nd-10 and Nd₂O₃ (inset in Fig. 4). Besides, the intensity of this wide Raman shift peak increases with an increase in the concentration of neodymium oxide in the Al₂O₃-Nd₂O₃ binary oxide as shown by the Al-Nd-10 binary oxide and PdO/Al-Nd-10 photocatalyst. This fact could explain the observed increase in the sizes of Nd₂O₃ nanocrystalline domains with the neodymium oxide concentration in the binary oxide. It is worthwhile to point out that the Raman shift peak observed at 1070 cm⁻¹ in the Al-Nd-10 binary oxide, PdO/Al-Nd-5 and PdO/Al-Nd-10 photocatalysts are not observed neither in the $\gamma\text{-Al}_2\text{O}_3$ nor in Nd₂O₃ (inset in Fig. 4). Thus, this Raman shift peak could arise from a new Nd³⁺ phase interacting with $\gamma\text{-Al}_2\text{O}_3$. Furthermore, the appearance of a mayor number of Raman shift peaks corresponding to Nd₂O₃ in the PdO/Al-Nd-10 photocatalyst suggests the presence of a mayor number of energetic molecular excitations in this material as compared to those of the PdO/Al-Nd-2 and PdO/Al-Nd-5 photocatalysts.

3.3. Optical properties of Pd/Al₂O₃-Nd₂O₃ photocatalysts

Fig. 5 shows the UV-vis spectra of $\gamma\text{-Al}_2\text{O}_3$, Nd₂O₃, Al-Nd-5 binary oxide, PdO/Al, PdO/Nd and PdO/Al-Nd-x photocatalysts. The UV-vis spectra of $\gamma\text{-Al}_2\text{O}_3$ and Al-Nd-5 binary oxide show a small absorption band at a wavelength of 290 nm. Whereas, the PdO/Al photocatalyst exhibits intensive absorption bands with a maximum at 212 and 370 nm as well as a weak signal at 255 nm, and an absorption edge in the visible region at wavelengths higher than 400 nm. Apparently, the signals observed at low wavelengths ($\lambda = 212$ and

255 nm) correspond to Pd²⁺ electronic states or highly dispersed PdO particles [29]. This we believe is valid given these absorption bands are not observed in $\gamma\text{-Al}_2\text{O}_3$, Al-Nd-5 binary oxide or Nd₂O₃ (inset in Fig. 5) and must correspond to the presence of PdO species requiring a higher energy for their electronic transitions. Thereby, it is inferred that such absorption bands may be attributed to Pd²⁺ states of highly dispersed PdO particles that are interacting strongly with the $\gamma\text{-Al}_2\text{O}_3$ support. Whereas, the absorption band at 370 nm and the absorption edge observed in the visible region at wavelengths higher than 400 nm are attributed to d-d transitions in Pd²⁺ states corresponding to the semi-conductive electronic structure of crystalline PdO [29,30]. The UV-vis spectra of the PdO/Al-Nd-2, PdO/Al-Nd-5 and PdO/Al-Nd-10 photocatalysts also show absorption bands corresponding to the electronic transitions of PdO species observed in PdO/Al. However, in addition, some absorption bands appear at wavelengths of 240, 580 and 744 nm. By comparison with the UV-vis spectra of the Al-Nd-5 binary oxide, PdO/Nd and Nd₂O₃ (inset in Fig. 5), it is inferred that these absorption bands must correspond to electronic transitions of the "f" orbitals of Nd³⁺ in Nd₂O₃ from the $^4\text{I}_{9/2}$ level ($4f^3$) to higher energy levels [16,31]. Besides, the absorption bands of the Nd³⁺ transitions observed at 580 and 744 nm in Nd₂O₃ (inset in Fig. 5) and PdO/Nd are shifted an about of 10–20 nm to lower wavelengths in the Al-Nd-5 binary oxide and PdO/Al-Nd-x photocatalysts. This shifting in the absorption bands to lower wavelengths in the photocatalytic materials based on Al₂O₃-Nd₂O₃ binary oxides suggests that a higher energy is required for the electronic transitions of Nd³⁺ due to the overlapping of the "4f" orbitals of Nd³⁺ in Nd₂O₃ with the "3p" orbitals of Al³⁺ in $\gamma\text{-Al}_2\text{O}_3$. On the hand, the absorption band of the Pd²⁺ electronic states observed at a wavelength of 370 nm in the UV-vis spectra of PdO/Al is shifted to the violet for about 30 nm in the PdO/Al-Nd-x photocatalysts. This observation suggests that a lesser energy is required for the Pd²⁺ electronic transitions due to the overlapping of the "4f" orbitals of Nd³⁺ with the "3p" orbitals of Al³⁺ forming hybridized orbitals with the "4d" orbitals of Pd²⁺ in PdO.

3.4. The photocatalytic degradation of phenol in aqueous medium

Earlier studies concerning to the photocatalytic efficiency of PdO/Al-Nd catalysts in the photodegradation of phenol showed that phenol molecules in aqueous medium (80 ppm) were not photodegraded neither by using UV electromagnetic radiation only ($\lambda = 254$ nm) nor with TiO₂-P25 (Degussa) as reference catalyst. The behavior of phenol molecules in aqueous medium during photolysis is shown in Fig. 6. It is observed that the molecule is not mineralized via photolysis since $\pi \rightarrow \pi^*$ transitions are preserved as shown by the absorption band at $\lambda = 270$ nm. The increase in the intensity of the absorption band at this wavelength indicates that phenol molecules are transformed to some intermediates species only by effect of the electromagnetic radiation. On the other hand, the photocatalytic activity test in the phenol photodegradation using TiO₂-P25 (Degussa) showed a conversion of 26% after 6 h under UV irradiation (Table 2). Higher efficiency in the photodegradation of phenol molecules is observed when the photocatalytic activity test is carried out by using PdO supported on $\gamma\text{-Al}_2\text{O}_3$ (PdO/Al) and PdO supported on Al₂O₃-Nd₂O₃ (PdO/Al-Nd-x) as shown by the absorption band at $\lambda = 270$ nm in the UV-vis spectra of the irradiated phenol dissolutions (Fig. 7). It can be observed that after 6 h of UV irradiation (Table 2, cycle 1), the photoconversion of phenol is increased in the sequence PdO/Al (38.0%), PdO/Al-Nd-2 (57.0%), PdO/Al-Nd-5 (63.0%) and PdO/Al-Nd-10 (75.0%). On the other hand, in order to study the adsorption capacity of the materials before irradiation with UV light, all solutions were continuously stirred without UV irradiation (dark light) during 1 h. As evidenced

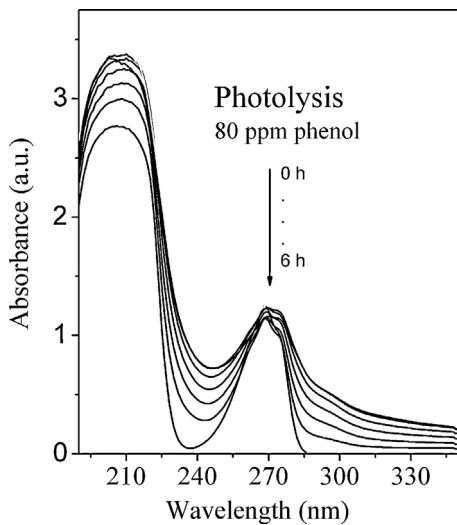


Fig. 6. UV-vis spectra of the aqueous phenol dissolution (80 ppm) after photolysis during 6 h.

in Fig. 8, the change in the relative C/C_0 concentration of phenol is negligible without UV irradiation, indicating adsorption phenomena are not occurring before irradiation starts. As it can be observed the relative C/C_0 amount of phenol decrease uniformly with the time of UV irradiation as well as with the increase in the concentration of Nd_2O_3 in the PdO/Al-Nd photocatalysts, being PdO/Al-Nd-10 the material that has the highest efficiency in the elimination of phenol after 6 h of UV irradiation. This result showed that the PdO/Al-Nd-10 photocatalyst is nearly three times more active than TiO_2 -P25 as reference catalyst.

The kinetic of photodegradation of phenol over the PdO/Al-Nd photocatalysts was fitted to a pseudo first-order equation using the Langmuir-Hinshelwood model [11,32], which is commonly used to describe the kinetics of photocatalytic reactions of organic compounds in aqueous solutions. The half-life time ($t_{1/2}$) of photodegraded phenol is calculated by plotting $\ln(C_0/C)$ versus reaction time (t) by the equation (1):

$$\ln(C_0/C) = K_{\text{app}}t \quad (1)$$

where K_{app} is an apparent rate constant defined by $K_{\text{app}} = k_r K_{\text{ad}}$ and k_r is the intrinsic rate constant while K_{ad} is the adsorption equilibrium constant. The plots of $\ln(C_0/C)$ versus reaction time (inset in Fig. 8) for PdO/Al and PdO/Al-Nd photocatalysts exhibit straight lines indicating that phenol photodegradation reaction adjusts well to a pseudo-first-order kinetics. The half-life time ($t_{1/2}$) values and the percentage of eliminated phenol are shown in Table 2. A decrease in the half-life time and in the pollutant concentration is observed with the increase of Nd_2O_3 in the materials. In contrast, a long-life time is observed when TiO_2 -P25 is used as reference catalyst (Table 2).

Table 2

Photocatalytic behavior: half life time and % of photodegradation of phenol after 6 h of UV irradiation.

Photocatalyst	% Nd_2O_3	$t_{1/2}$ (h)	Phenol photodegradation (%)	
			Cycle 1	Cycle 2
PdO/Al	0	8.9	38.0	27.0
PdO/Al-Nd-2	2	5.1	57.0	76.0
PdO/Al-Nd-5	5	4.7	63.0	77.0
PdO/Al-Nd-10	10	3.3	75.0	78.0
TiO ₂ -P25 (Degussa)	–	12.0	26.0	–

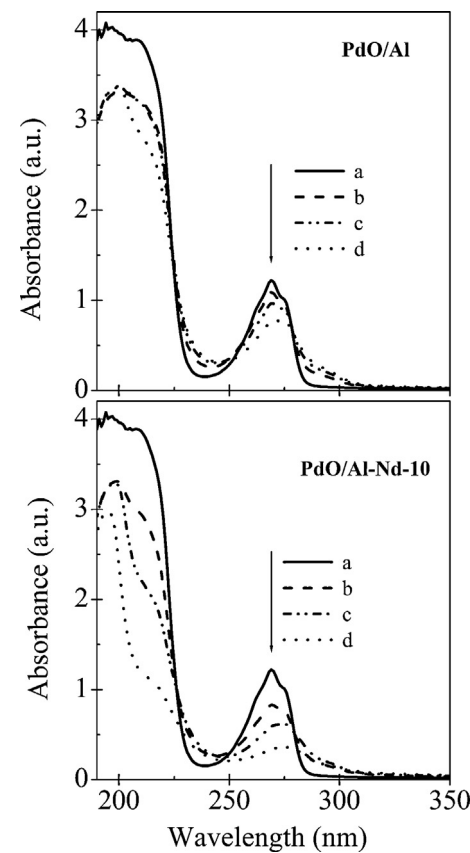


Fig. 7. UV photodegradation of phenol in aqueous medium over PdO/Al₂O₃ and PdO/Al-Nd-10 photocatalysts after: (a) 0 h of irradiation; (b) 2 h of irradiation; (c) 4 h of irradiation; and (d) 6 h of irradiation.

On the other hand, the effect of the sample weight of photocatalyst on the reaction rate constant in the photodegradation of phenol over PdO/Al-Nd-5 and PdO/Al-Nd-10 samples is shown in Fig. 9. It is observed an increase in the reaction rate constant with the increase in the sample weight of photocatalyst after 6 h of UV irradiation. The linearity observed at low photocatalyst weights indicate

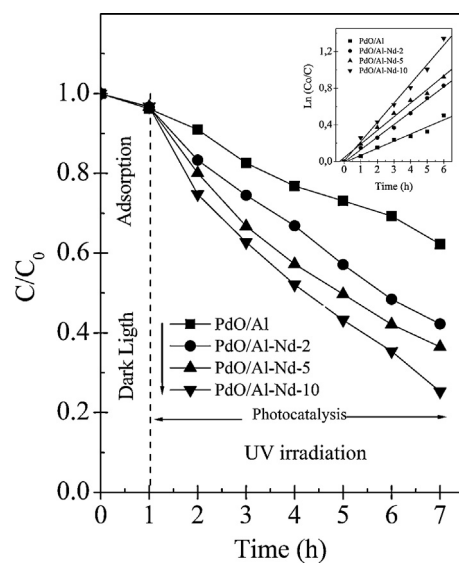


Fig. 8. Relative concentration (C/C_0) of phenol versus irradiation time over PdO photocatalysts supported on Al₂O₃-Nd₂O₃ binary oxides. Inset plot: $\ln(C_0/C)$ versus reaction time (t).

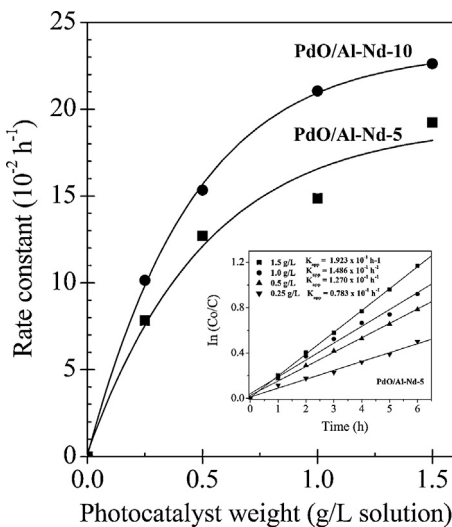


Fig. 9. Rate constant values as a function of the photocatalyst weight (g/L) after 6 h of UV irradiation. Inset plot: $\ln(C_0/C)$ versus reaction time (t) for photocatalyst weights in the range 0.5–1.5 g/L of aqueous phenol dissolution.

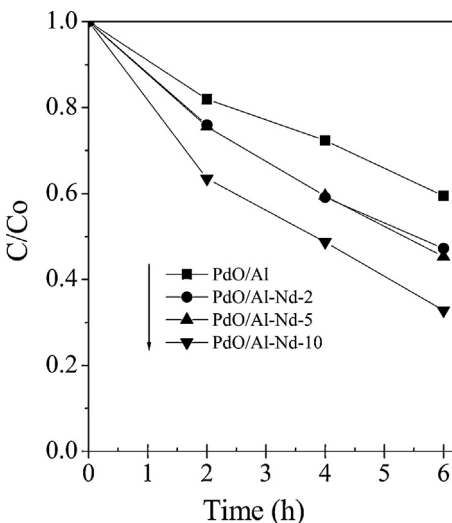


Fig. 10. Total organic carbon (TOC) of the phenol dissolution versus irradiation time over PdO photocatalysts supported on $\text{Al}_2\text{O}_3\text{-Nd}_2\text{O}_3$ binary oxides.

that diffusional effects caused by reflected light or reactant medium opacity due to the suspended particles are not present at these concentrations. In our case we use 1.0 g/L of solid for the photoactivity test which is nearly the limit where the maximum efficiency of the photocatalysts in the photodegradation of phenol is reached. The plots of $\ln(C_0/C)$ versus reaction time (inset in Fig. 9) for the selected PdO/Al-Nd-5 photocatalyst in the range 0.25–1.5 g/L of aqueous phenol dissolution exhibit straight lines plots indicating a lineal tendency between the reaction rate constant and the photocatalyst sample weight.

The total organic carbon analysis (TOC) of irradiated solutions is shown in Fig. 10. It is observed a continuous decrease of organic carbon indicating a high mineralization of phenol. The photocatalytic activity in the photodegradation of phenol over the recovered photocatalysts samples after the first cycle of reaction is shown in Table 2. The photoconversion of phenol on the recovered PdO/Al photocatalyst in the second cycle of reaction (~27.0%) is lower than that of the first cycle of reaction (~38.0%), while when the second cycle of reaction is carried out over the recovered PdO/Al-Nd photocatalysts the photocatalytic efficiency is improved with the

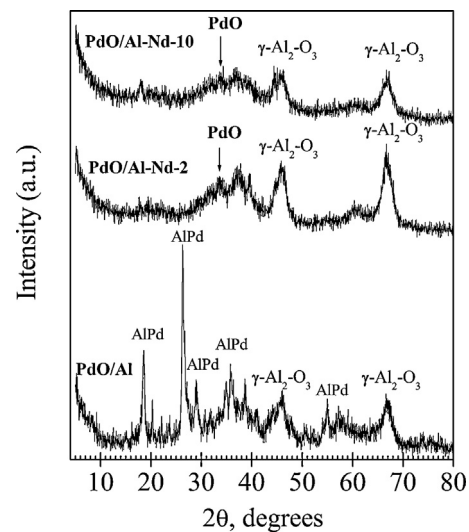


Fig. 11. X-ray diffraction patterns of the recovered solids from the remaining aqueous phenol – photocatalyst dissolution after the first cycle of reaction.

irradiation time attaining about 76.0–78.0% of phenol photoconversion after 6 h of UV irradiation (Table 2).

The XRD patterns of the recovered solids after UV irradiation are shown in Fig. 11. It can be observed that the XRD patterns of recovered PdO/Al-Nd photocatalysts after the first cycle of reaction are similar to those measured before UV irradiation (Fig. 3) [13]. However, the XRD pattern of the recovered PdO/ $\gamma\text{-Al}_2\text{O}_3$ photocatalyst, after the first cycle of reaction, is clearly different from the one obtained before UV irradiation since in addition to the diffraction peaks at $2\theta=45.9^\circ$ and 66.8° corresponding to the $\gamma\text{-Al}_2\text{O}_3$, some extra diffraction peaks appear at $2\theta=18.4^\circ$, 26.3° , 29.0° , 35° and 38.5° . The identification of these diffraction peaks according to the 31-27 JCPDS card is nearly consistent with the presence of an AlPd alloy compound. This observation suggests that the PdO/ Al_2O_3 photocatalyst may undergo a partial transformation into PdAl alloy species when irradiated with UV light. The formation of PdAl alloy species has been also observed after reduction of Pd/ Al_2O_3 catalysts in hydrogen at 600°C for 17 h [33]. An abundant presence of $\gamma\text{-Al}_2\text{O}_3$ agglomerates covering the PdO surface should enhance the interaction between PdO crystallites and $\gamma\text{-Al}_2\text{O}_3$ forming a PdO- Al_2O_3 interface. Thereby, the UV irradiation could reduce locally the PdO- Al_2O_3 interface forming Pd-Al alloy species. In contrast, the structure of PdO/Al-Nd photocatalysts is preserved after UV irradiation indicating the addition of Nd₂O₃ to $\gamma\text{-Al}_2\text{O}_3$ stabilizes the structure of PdO crystallites.

The improved photocatalytic activity of PdO/Al-Nd photocatalysts could be due to an important interaction between PdO crystallites and Nd₂O₃ microcrystalline domains that are homogeneously well mixed with the $\gamma\text{-Al}_2\text{O}_3$ agglomerates. The enhancement of the photocatalytic activity in the degradation of phenol with Nd₂O₃ concentration in the $\text{Al}_2\text{O}_3\text{-Nd}_2\text{O}_3$ binary oxides is correlated with an increase in the size of the Nd₂O₃ microcrystalline domains that are interacting with the $\gamma\text{-Al}_2\text{O}_3$. Therefore, the improvement in the photocatalytic activity of PdO/Al-Nd photocatalysts with Nd₂O₃ concentration could be related to the presence of a major number of energetic molecular excitations in the materials (electron/hole pairs) as compared to that of PdO/ Al_2O_3 photocatalyst. Such interaction between $\gamma\text{-Al}_2\text{O}_3$ agglomerates and Nd₂O₃ microcrystalline domains increases with the Nd₂O₃ content and it is expected that a new phase of Nd³⁺ interacting with $\gamma\text{-Al}_2\text{O}_3$ could be formed giving rise to a higher number of e⁻ and h⁺ pairs that could interact with the empty Pd 4d states of the PdO conduction band. This could be so because

less energy is required for the Pd^{2+} electronic transitions to occur due to the overlapping of the “4f” orbitals of Nd^{3+} in Nd_2O_3 with the “3p” orbitals of Al^{3+} in $\gamma-Al_2O_3$ forming hybridized orbitals with the “4d” orbitals of Pd^{2+} in the PdO crystallites. Therefore, the PdO semiconductor properties in the $PdO/\gamma-Al_2O_3$ photocatalysts can be improved by the addition of Nd_2O_3 in the $\gamma-Al_2O_3$ support. Furthermore, the overlapping of different orbitals by coupling $\gamma-Al_2O_3-Nd_2O_3$ binary oxides and PdO could decrease the recombination rate of the charge carriers of the PdO semiconductor. A good combination of the conduction and valence bands levels of $\gamma-Al_2O_3$, Nd_2O_3 and PdO could generate a higher transfer of photogenerated charge carriers improving the photocatalytic efficiency of the $PdO/\gamma-Al_2O_3$ photocatalyst.

4. Conclusions

$PdO/\gamma-Al_2O_3$ photocatalyst is capable of photodegrading phenol in aqueous medium. The incorporation of Nd_2O_3 to $\gamma-Al_2O_3$ by means of the sol-gel method improves the photocatalytic activity and stabilizes the structure of the PdO photocatalysts. PdO photocatalysts exhibit a higher efficiency in the elimination of phenol with an increase of Nd_2O_3 concentration in the $\gamma-Al_2O_3-Nd_2O_3$ support. When the concentration of Nd_2O_3 in the binary oxide reaches 10 wt%, photodegradation of phenol as well as the decrease in the dissolved organic carbon is highly enhanced. The photocatalytic activity in the degradation of phenol by using the recovered $PdO/Al-Nd$ photocatalysts is preserved after reaction. The observed improvement in the photocatalytic activity of $PdO/Al-Nd$ photocatalysts can be due to an important interaction between the highly dispersed PdO nano-crystallites and the Nd_2O_3 microcrystalline domains that are homogeneously well mixed with the $\gamma-Al_2O_3$.

Acknowledgments

This work was supported partially by grants from COECYT-JAL (Project: 06-200732), CONACYT (Projects: 60702, 119058), and PROMEP; J.E. Casillas is indebted to CONACYT for his scholarship granted (CONACYT scholar No. 287873).

References

- [1] G. Busca, S. Berardinelli, C. Resini, L. Arrighi, J. Hazard. Mater. 160 (2008) 265–288.
- [2] N.H. Salah, M. Bouhelassa, S. Bekkouche, A. Boultif, Desalination 166 (2004) 347–354.
- [3] S. Esplugas, J. Gimenez, S. Contreras, E. Pascual, M. Rodríguez, Water Res. 36 (4) (2002) 1034–1042.
- [4] V. Belessi, D. Lambropoulou, I. Konstantinou, A. Katsoulidis, P. Pomonis, D. Petridis, T. Albanis, Appl. Catal. B 73 (2007) 292–299.
- [5] C.-H. Chiou, C.-Y. Wu, R.-S. Juang, Chem. Eng. J. 139 (2008) 322–329.
- [6] B. Pourabbas, B. Jamshidi, Chem. Eng. J. 138 (2008) 55–62.
- [7] E. Rodríguez, G. Fernández, B. Ledesma, P. Álvarez, F.J. Beltrán, Appl. Catal. B 92 (2009) 240–249.
- [8] F.B. Li, X.Z. Li, X.M. Li, T.X. Liu, J. Dong, J. Colloid Interface Sci. 311 (2007) 481–490.
- [9] F.B. Li, X.Z. Li, C.S. Liu, X.M. Li, T.X. Liu, Ind. Eng. Chem. Res. 46 (2007) 781–787.
- [10] A. Patzko, R. Kun, V. Hornok, I. Dekany, T. Engelhardt, N. Schall, Colloid Surf. A 265 (2005) 64–72.
- [11] J.S. Valente, F. Tzompantzi, J. Prince, J.G.H. Cortez, R. Gómez, Appl. Catal. B 90 (2009) 330–338.
- [12] A. Mantilla, F. Tzompantzi, J.L. Fernández, J.A.I. Díaz Góngora, R. Gómez, Catal. Today 150 (2010) 353–357.
- [13] A. Barrera, F. Tzompantzi, V. Lara, R. Gómez, J. Photochem. Photobiol. A: Chem. 227 (2012) 45–50.
- [14] J.R. McBride, K.C. Hass, W.H. Weber, Phys. Rev. B 44 (10) (1991) 5016–5028.
- [15] Y. Ozawa, Y. Tochihara, M. Nagai, S. Omi, Catal. Commun. 4 (2003) 87–90.
- [16] F. Oudet, P. Courtine, A. Vejux, J. Catal. 114 (1988) 112–120.
- [17] U.G. Akpan, B.H. Hameed, Appl. Catal. A 375 (2010) 1–11.
- [18] T.L.R. Hewer, E.C.C. Souza, T.S. Martins, E.N.S. Muccillo, R.S. Freire, J. Mol. Catal. A: Chem. 336 (2011) 58–63.
- [19] Y.H. Xu, C. Chen, X.L. Yang, X. Li, B.F. Wang, Appl. Surf. Sci. 255 (2009) 8624–8628.
- [20] B. Shahmoradi, I.A. Ibrahim, N. Sakamoto, S. Ananda, R. Somashekar, T.N. Guru Row, K. Byrappa, J. Environ. Sci. Health A: Toxic/Hazard. Subst. Environ. Eng. 45 (2010) 1248–1255.
- [21] D. de la Cruz Romero, G. Torres Torres, J.C. Arévalo, R. Gómez, A. Aguilar-Elguezabal, J. Sol-Gel Sci. Technol. 56 (2010) 219–226.
- [22] F. Galindo-Hernández, R. Gómez, J. Photochem. Photobiol. A 217 (2011) 383–388.
- [23] R. López, R. Gómez, M.E. Llanos, Catal. Today 148 (2009) 103–108.
- [24] V. Rodríguez-González, M.A. Ruiz-Gómez, L.M. Torres-Martínez, R. Zanella, R. Gómez, Catal. Today 148 (2009) 109–114.
- [25] X. Quan, Q. Zhao, H. Tan, X. Sang, F. Wang, Y. Dai, Mater. Chem. Phys. 114 (2009) 90–98.
- [26] V. Rodríguez-González, A. Moreno-Rodríguez, M. May, F. Tzompantzi, R. Gómez, J. Photochem. 193 (2008) 266–270.
- [27] A.-Ch. Lee, R.-H. Lin, Ch.-Y. Yang, M.-H. Lin, W.-Y. Wang, Mater. Chem. Phys. 109 (2008) 275–280.
- [28] S. Lowell, J.E. Shields, M.A. Thomas, in: M. Thommes (Ed.), Characterization of porous solids and powders: surface area, Pore Size and Density, Springer, Netherlands, 2004, pp. 31–32.
- [29] A.N. Pestyakov, V.V. Lunin, S. Fuentes, N. Bogdanchikova, A. Barrera, Chem. Phys. Lett. 367 (2003) 102–108.
- [30] M. Lyubosky, L. Pfefferle, Catal. Today 47 (1997) 29–44.
- [31] P. Caro, Structure Électronique des Éléments de Transition, 1st ed., Presses Universitaires de France, Paris, 1976.
- [32] K. Porkodi, K.V. Kumar, Appl. Catal. B 79 (2008) 108–109.
- [33] M. Skotak, Z. Karpinski, W. Juszczuk, J. Pielaszek, L. Kepinski, D.V. Kazachkin, V.I. Kovalchuk, J.L. d'Itri, J. Catal. 227 (2004) 11–25.